International Journal of Geo-Information

MDPI

Article

Automatic Parametrization of Urban Areas Using ALS Data: The Case Study of Santiago de Compostela

Mario Soilán [1,*], Belén Riveiro [1], Patricia Liñares [2] and Andrea Pérez-Rivas [2]

[1] Department of Materials Engineering, Applied Mechanics and Construction, School of Industrial Engineering, University of Vigo, 36310 Vigo, Spain; belenriveiro@uvigo.es

[2] Department of Natural Resources and Environmental Engineering, School of Mining Engineering, University of Vigo, 36310 Vigo, Spain; plinhares@uvigo.es (P.L.); andreaperezrivas24@gmail.com (A.P.-R.)

* Correspondence: msoilan@uvigo.es

Received: 9 October 2018; Accepted: 7 November 2018; Published: 9 November 2018

Abstract: Nowadays, gathering accurate and meaningful information about the urban environment with the maximum efficiency in terms of cost and time has become more relevant for city administrations, as this information is essential if the sustainability or the resilience of the urban structure has to be improved. This work presents a methodology for the automatic parametrization and characterization of different urban typologies, for the specific case study of Santiago de Compostela (Spain), using data from Aerial Laser Scanners (ALS). This methodology consists of a number of sequential processes of point cloud data, using exclusively their geometric coordinates. Three of the main elements of the urban structure are assessed in this work: intersections, building blocks, and streets. Different geometric and contextual metrics are automatically extracted for each of the elements, defining the urban typology of the studied area. The accuracy of the measurements is validated against a manual reference, obtaining average errors of less than 3%, proving that the input data is valid for this assessment.

Keywords: Aerial Laser Scanner; point cloud processing; classification; urban parametrization

1. Introduction

The sustainability of the urban environment is one of the biggest challenges of modern societies. The role played by cities in the global economy is obvious as they are our main form of habitat, and an essential pillar for the development of society. That is why there is an increasing awareness of the necessity to re-think the concept of the city. The United Nations Human Settlements Programme (UN-Habitat) [1] defines the 21st century city as sustainable (low energy consumption, small ecological footprint) [2–4] and resilient (reducing risks and vulnerabilities, designing adequate infrastructures) [5–7]. Traditional approaches of urban management are inadequate nowadays, so experimenting with new approaches and solutions, as well as developing a greater interaction between researchers from different fields and municipalities is essential to find the most efficient ways to evolve from traditional cities to those described by the UN-Habitat [8].

Accordingly, the usage of data acquisition technologies that allow an efficient collection of urban data is fundamental for developing new strategies of urban planning as well as for assessing the existing urban infrastructure. Thus, two data sources can be highlighted. On one side, satellite imagery has been used for a large number of applications. Some examples are the analysis of urban hazards [9,10], the segmentation of urban features [11,12], or shadow detection [13], among others. On the other side, laser scanner technology has been used in multiple research fields during the last decade, and it is proven to be a useful tool for a wide number of applications that may have an impact on the evolution of the sustainability and resilience of the cities. Laser scanners are able to

collect geomatic data in an accurate and efficient manner, in the form of 3D point clouds, which are unorganized sets of 3D coordinates with a number of radiometric and contextual parameters assigned to them. According to the acquisition system, the literature regarding the application of laser scanning data to assess urban issues can be divided in two categories. First, Terrestrial Laser Scanners (TLS), typically integrated in mobile platforms [14], are mainly used for applications that require a detailed representation or the urban environment, such as urban object detection [15–19], where a number of common elements such as street lights, vehicles, bins, etc. are automatically classified for point cloud data; or infrastructure assessment [20–23], including the characterization and evaluation of pavement, road signage, and the structure of the building facades. The second category regarding the acquisition system is composed by Aerial Laser Scanner (ALS) applications. These systems are able to collect data from large surfaces in much less time than a terrestrial system, but the spatial resolution of the resulting point clouds is considerably smaller. However, it is enough for a wide range of applications, such as roof extraction and parametrization [24,25] or urban vegetation assessment [26,27]. Of special interest for this manuscript is the usage of ALS technology for urban parametrization. Hermosilla et al. [28] used high-spatial resolution imagery and aerial LiDAR data to define urban typologies based on a partition of the public street space, which was related to urban blocks, for the case study of Valencia (Spain). Similarly, Vanderhaegen and Canters [29] define a set of urban metrics for the case study of Brussels (Belgium) that are used to classify six land-use/urban-form (LUUF) classes.

This work presents a methodology for the automatic parametrization of urban areas for the case study of Santiago de Compostela (Spain). The main contribution of this work is the development of methodologies that exclusively employ the geographic coordinates (x,y,z) of aerial point clouds, in order to obtain geometric and contextual parameters of three main urban elements: intersections, building blocks, and streets, and to prove that aerial point clouds with rather small densities are suitable for applications that aim to define urban typologies in different scales.

The paper is structured as follows. In Section 2, the methodology is presented in detail. Section 3 shows the case study data, where the methodology has been applied and validated. Section 4 shows the results of the urban parametrization, as well as validation data where these parameters are compared with a manual reference. Section 5 presents the conclusions of the work.

2. Methodology

This section presents the developed methodology for urban parametrization as a sequential application of point cloud processing algorithms which takes as input a raw point cloud of an urban area and outputs a set of geometric parameters describing streets, building blocks, and intersections, as depicted in Figure 1.

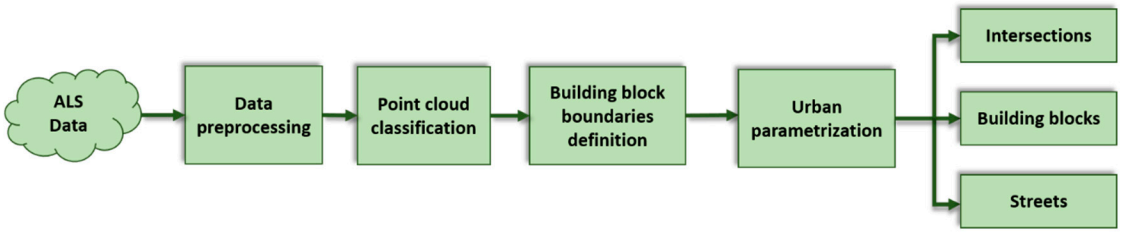

Figure 1. Methodology workflow.

2.1. Data Preprocessing

Let $\boldsymbol{P} = (\boldsymbol{x}, \boldsymbol{y}, \boldsymbol{z})$ be a raw 3D point cloud, defined as a N × 3 matrix where N is the number of points and $(\boldsymbol{x_i}, \boldsymbol{y_i}, \boldsymbol{z_i})$ are the coordinates of the point $\boldsymbol{i} \mid \boldsymbol{0} < \boldsymbol{i} \leq \boldsymbol{N}$. In first place, the point cloud has to be classified in two main groups: Ground and roofs. Note that, as the spatial resolution of the point cloud is too small (see Section 3), points in facades are sparse and occlusions are likely to happen, hence they will not provide reliable information for the parametrization of the urban area. Therefore,

this preprocessing stage consists of the application of a filter that removes points that do not belong to the ground or to the roofs. This filter is based on the normal vector of the points in $\boldsymbol{P}$. For each point, a spherical neighborhood of 6 meters is computed (this neighborhood criteria has proven to be valid in previous work [25]), obtaining the coordinates of M neighbors, and Principal Component Analysis (PCA) is applied over the M $\times$ 3 covariance matrix defined by the coordinates of these M neighbors. The normal vector of the point is defined as the third eigenvector retrieved by PCA, which corresponds to the smallest eigenvalue [30]. Then, the coordinates of this vector are transformed into spherical coordinates (azimuth angle, elevation angle, radius). The elevation coordinate represents the angle with respect to the x-y plane, therefore, both ground and roof points will have elevations around 90 degrees, while the elevation of vertical structures will be close to 0 (Figure 2a). Using a single threshold is enough to filter out points from vertical structures. Here, points whose normal vector has an elevation angle less than 15 degrees (being this a soft threshold that has into consideration the possibility of inclined areas) are filtered out from the point cloud $\boldsymbol{P}$ (Figure 2b). Let $\boldsymbol{P_p} = (\boldsymbol{x}, \boldsymbol{y}, \boldsymbol{z})$ be the preprocessed point cloud that is obtained after the application of this step.

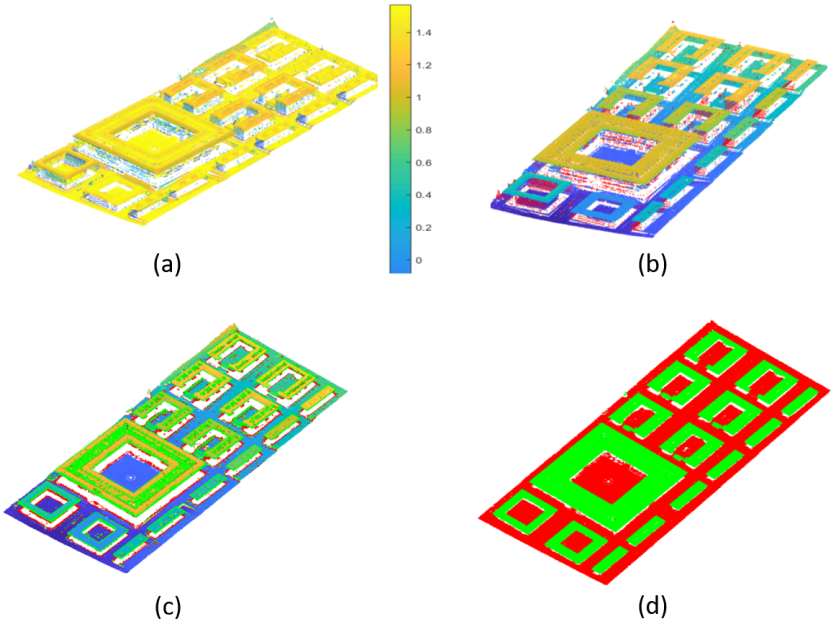

Figure 2. Point cloud classification. (**a**) Point cloud coloured by elevation. (**b**) Elevation-based filtering. Points that do not belong to roofs or to the ground are removed from the point cloud. (**c**) After performing the triangulation T_{Pp}, two groups of points are labelled as either ground or roof. (**d**) A region growing algorithm classifies the complete point cloud.

2.2. Point Cloud Classification

Once the point cloud has been preprocessed, the next step aims at classifying the two main groups of points that remain in the cloud: ground and roofs. This process has some similarities with regard to previous work [25]. First, a Delaunay Triangulation $\boldsymbol{T_{Pp}}$ (a Triangulation $\boldsymbol{T_p}$ is a N $\times$ 3 matrix representing sets of three point indices in the point cloud P that form a triangle whose circumcircle do not contain any other point) is computed on $\boldsymbol{P_p}$ [31]. As vertical structures have been removed in the previous step, it is straightforward to find which triangles connect the ground and the roofs as those whose normal vector has an angle with respect to the vertical (that is, with respect to Z-axis) larger than a threshold $\beta = 55°$ (again, this threshold considers the possibility of inclined areas) and whose height difference between the highest and the lowest point is larger than $h = 3$ m. For every triangle that complies with these conditions, which were initially defined in [25], the highest and the lowest point are labeled as roof point and ground point, respectively (Figure 2c).

Then, the triangles that were selected in the previous step are removed from the triangulation $\boldsymbol{T_{Pp}}$. This way, with no connections between ground and roofs, it is possible to classify every point in the cloud as either ground or roof. Starting from labeled points, a region growing algorithm assigns labels to every point in the cloud, taking into consideration the presence of vegetation or other artifacts. This process, which is explained in detail in [25], outputs two point clouds, $\boldsymbol{P_r}$ containing the roofs, and $\boldsymbol{P_g}$ containing the ground, such that $\boldsymbol{P_r} \cap \boldsymbol{P_g} = \varnothing$ (Figure 2d).

2.3. Bulding Block Boundaries

Given the point cloud $\boldsymbol{P_r}$ of points that belong to building roofs, it is possible to define the bulding blocks in the studied area. A building block is simply defined as an edification (or group of edifications) that is surrounded by the ground, and for this work, it will be represented as a group of points $\boldsymbol{B_i} = (\boldsymbol{x}, \boldsymbol{y}, \boldsymbol{z})_i \mid \boldsymbol{B_i} \in \boldsymbol{P_r}$ that conform to the boundaries of the block. In order to get these building blocks, the 3D information of $\boldsymbol{P_r}$ is rasterized in a first place, that is, the points of the cloud are projected on the XY plane where a square grid of size $g_s = 1.5$ m is defined, and each point is assigned to the cell within the grid where it is projected. Then, a binary image $\boldsymbol{I_b}$ can be constructed, assuming that there are cells with no points (black pixels) and cells with at least one point (white pixels), as it can be seen in Figure 3a. Once $\boldsymbol{I_b}$ is built, it is necessary to process it to improve the building block representation quality: There are several holes due to either the small density of the point cloud or occlusions, and it is also mandatory to distinguish between exterior and interior boundaries within the same building block. To solve the first problem, a NOT operation is applied to $\boldsymbol{I_b}$ (Figure 3b), and a connected components algorithm is applied to the resulting image $(\overline{\boldsymbol{I_b}})$. Small holes in $\boldsymbol{I_b}$ are equivalent to elements with only a few pixels in the connected components data from $\overline{\boldsymbol{I_b}}$. Elements with less than 10 pixels are selected as holes and converted to white in the image $\boldsymbol{I_b}$. Finally, the Moore–Neighbor tracing algorithm modified by Jacob's stopping criteria [32] is applied in order to select pixels that belong to internal and external boundaries (Figure 3c). Then, the pixel indices from each external boundary can be used to retrieve the 3D coordinates of the correspondent points in $\boldsymbol{P_r}$, defining the boundaries $\boldsymbol{B_i}$. Regarding the internal boundaries, they are analogously defined as $\boldsymbol{IB_j} = (\boldsymbol{x}, \boldsymbol{y}, \boldsymbol{z}, \boldsymbol{id})_j$, where $\boldsymbol{id}$ is an index that relates an internal boundary to a building block, that is, an internal boundary with $id = k$ will be part of the building whose external boundary is $\boldsymbol{B_k}$.

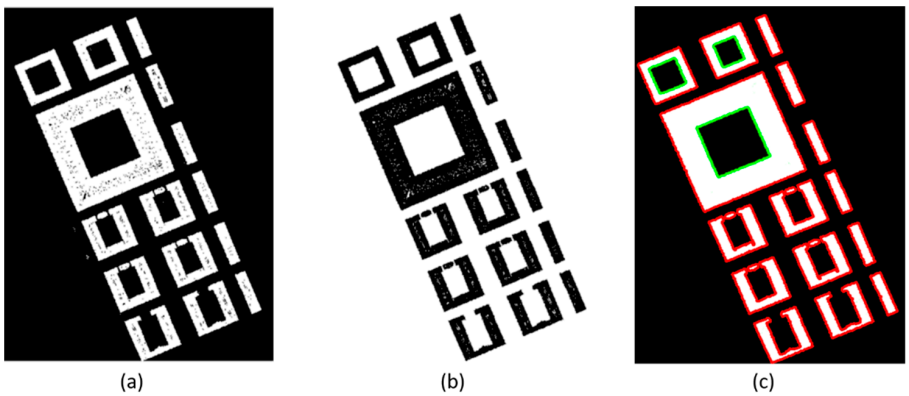

Figure 3. Building block boundaries. (**a**) Raster image of the point cloud $\boldsymbol{P_r}$ $(\boldsymbol{I_b})$. (**b**) Image $\overline{\boldsymbol{I_b}}$, defined to remove noisy elements. (**c**) External and internal building boundaries, coloured in red and green, respectively.

2.4. Intersections, Streets, and Building Blocks

The information regarding building block boundaries is particularly useful for extracting the three elements that will be parametrized: intersections, streets, and building blocks. Assuming that the previous step resulted in N building block boundaries, a triangulation $\boldsymbol{T_B}$, where $\boldsymbol{B} = \cup_{i=1}^{N} \boldsymbol{B_i}$ (that is, the union of all the building block boundaries) is defined. Then, the vertices of each triangle

$(\boldsymbol{p_1}, \boldsymbol{p_2}, \boldsymbol{p_3})$ within $\boldsymbol{T_B}$ are analyzed, considering three possible options: (1) Each vertex belong to a different boundary, $\boldsymbol{p_1} \in \boldsymbol{B}_i$, $\boldsymbol{p_2} \in \boldsymbol{B}_j$, $\boldsymbol{p_3} \in \boldsymbol{B}_k \mid i \neq j \neq k$. (2) Two of the vertices belong to the same boundary, $\boldsymbol{p_1}, \boldsymbol{p_2} \in \boldsymbol{B}_i$, $\boldsymbol{p_3} \in \boldsymbol{B}_j \mid i \neq j$. (3) All the vertices belong to the same boundary, $\boldsymbol{p_1}, \boldsymbol{p_2}, p_3 \in \boldsymbol{B_i}$. As can be seen in Figure 4, each group of triangles will clearly represent building blocks, streets, and intersections.

For the first case, whenever the vertices of a triangle belong to three different building block boundaries, they are defined as intersections. As more than one triangle may belong to the same intersection, it is necessary to check whether or not each intersection triangle from $\boldsymbol{T_B}$ has vertices in common with the other intersection triangles. If two triangles have two vertices in common, they will be defined as part of the same intersection. Finally, intersections are defined as a set of point clouds $\boldsymbol{In} = \{\boldsymbol{In_1}, \ldots \boldsymbol{In_i}, \ldots \boldsymbol{In_n}\}$, where $\boldsymbol{In_i} \in \boldsymbol{B}$.

When the vertices of a triangle belong to two different building block boundaries, they are defined as streets. Note that streets defined in this way do not need to match contextually with the actual streets on the map, but this representation is useful for their parametrization, as can be seen in Section 2.5. Streets are defined as a set of point clouds $\boldsymbol{St} = \{\boldsymbol{St_1}, \ldots \boldsymbol{St_2}, \ldots \boldsymbol{St_3}\}$ where $\boldsymbol{St_i} \in \boldsymbol{B_i} \cup \boldsymbol{B}_j \mid i \neq j$.

Finally, when the vertices of a triangle all belong to the same building block boundary, they are defined as building blocks. Analogously to the previous elements, a building block is defined as $\boldsymbol{Bk} = \{\boldsymbol{Bk_1}, \ldots, \boldsymbol{Bk_i}, \ldots, \boldsymbol{Bk_n}\}$ where $\boldsymbol{Bk_i} \in \boldsymbol{B_i}$.

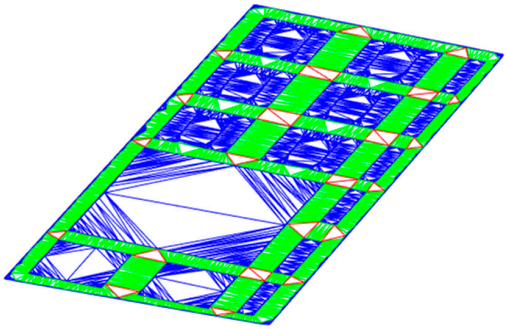

Figure 4. Triangulation $\boldsymbol{T_B}$, where each triangle is coloured according to the number of building blocks that are in contact with its vertices. Red triangles are in contact with 3 blocks (intersections), green triangles are in contact with two blocks (streets) and blue triangles are in contact with only one block (building blocks).

2.5. Urban Parametrization

The information in $\boldsymbol{In}$, $\boldsymbol{St}$, and $\boldsymbol{Bk}$ can be used to extract a set of relevant parameters of the urban area:

Regarding intersections, the only geometric parameter that is considered is the surface of the intersection, which is simply defined as the addition of the area of each triangle resulting from the triangulation of $\boldsymbol{T_{In_i}}$. Then, contextual parameters are also stored. Both the indices of the blocks in $\boldsymbol{Bk}$ and the streets in $\boldsymbol{St}$ that are in contact with the intersection are stored as properties.

Building blocks and streets are defined with a richer set of properties than intersections. The parameters that define a building block are:

- Building block surface: The surface covered by the building block is computed in a similar fashion than for intersections. A triangulation is defined for each block in $\boldsymbol{Bk}$, and the surface is defined as the sum of the area of all the triangles within the triangulation.
- Building block height: In order to define the height of a building block, a set of four parameters are employed, namely average height, maximum height, minimum height, and height standard deviation. For each point in a building block $\boldsymbol{Bk_i}$, the vertical distance with respect to the closest point in the ground $(\boldsymbol{P}_g)$ is computed. These distances define a vector of heights $\boldsymbol{H}_b$, whose elements are used to compute the aforementioned parameters.

- Building block volume: The volume of the building block is estimated as the product of the surface and the average height of the block.
- Building block built surface: For each building block $\boldsymbol{Bk_i}$, the internal boundaries from $\boldsymbol{IB}$ that belong to the interior of $\boldsymbol{Bk_i}$ are retrieved. Then, the surface of the internal boundaries is computed, and substracted to the building block surface to get the built surface.
- Building block built volume: Similarly to the total volume of the block, the built volume is the product of the built surface and the average height.
- Facade orientation: An important parameter that defines a building block is the orientation of the facades. For each building block $\boldsymbol{Bk_i}$, an iterative process that approximates the points in $\boldsymbol{Bk_i}$ to a polyline (which is a set of vertices $L = \{\boldsymbol{G}_1, \boldsymbol{G}_2, \ldots, \boldsymbol{G}_n\} \mid \boldsymbol{G} \in \boldsymbol{Bk_i}$) is applied in a first place. This process follows the approach in [33]. The first vertex, $\boldsymbol{G}_1$ is selected randomly and the next vertex $\boldsymbol{G}_2$ is defined as the further neighbor in a sphere with a 5 m radius, obtaining the first line. The process is repeated until all the points are within the neighborhood of a vertex. The orientation of the façade can be estimated as a vector perpendicular to the unit vector of each line ($v_{GiGj} = \frac{Gi-Gj}{||Gi-Gj||}$). However, there are two possible vectors that are perpendicular to v_{GiGj} (let them be v_1 and v_2), so to define the correct orientation is not straightforward. For each line $\overline{G_iG_j}$, the 20 closest points of the ground ($\boldsymbol{P}_{gn} \in \boldsymbol{P}_g$) with respect to the first vertex of the line are retrieved, and the average distance between unit vectors $v_{G_iPgn_i}$ and v_1, v_2 is computed. As the orientation of the façade is such that the vector is oriented to the outside of the building, the vector with closest distance with the vectors that point to the ground will be chosen as the correct orientation for the façade (Equation). The orientation is finally represented with two parameters: the azimuth, which is the angle between the North (represented by the unit vector [1 0 0]) and the vector $v_\perp$, and an orientation label, which is one of the following: North East-South East, South East-South West, South West-North West, and North West-North East (Figure 5a).

$$if\ arg\min\left(\sum_i ||v_{G_iPgn_i} - v_1||, \sum_i ||v_{G_iPgn_i} - v_2||\right) = 1,\ v_\perp = v_1$$
$$else,\ v_\perp = v_2$$

The parameters defining streets are the following:

- Surface: It is computed following the same strategy than for intersections and building blocks, that is defining a triangulation for each street in $\boldsymbol{St}$ and adding up the area of all the triangles within the triangulation.
- Width: Similar to height in the case of building blocks, a total of four parameters are employed to define the width of each street: Average width, maximum width, minimum width, and width standard deviation. For each $\boldsymbol{St_i} \in \boldsymbol{B_i} \cup \boldsymbol{B_j} \mid i \neq j$, points that belong to one of the building blocks ($\boldsymbol{P_{Bi}}$) are selected. Then, a nearest neighbor search is performed for each point in $\boldsymbol{P_{Bi}}$ with respect to the points that belong to the remaining building block ($\boldsymbol{P_{Bj}}$), Figure 5b. The distances between each point in $\boldsymbol{P_{Bi}}$ and the closest point in $\boldsymbol{P_{Bj}}$ define a vector of street widths $\boldsymbol{W_s}$ which is used to compute the aforementioned parameters.
- Orientation: Recall that points in each $\boldsymbol{St_i}$ have been extracted from the building block boundaries in $\boldsymbol{B}$, hence they do not strictly represent the main axis of the street. However, this axis and the orientation of the streets can be retrieved from $\boldsymbol{St_i}$ points. As they belong to two different building blocks, it is straightforward to define two groups of points, let them be $\boldsymbol{P}_{b1}$ and $\boldsymbol{P}_{b2}$. Then, the nearest neighbor in $\boldsymbol{P}_{b2}$ for each point in $\boldsymbol{P}_{b1}$ is found and both points are averaged. Repeating this procedure for each point in $\boldsymbol{P}_{b1}$ results in a set of points that approximate the main axis of the street (Figure 5b). Finally, an orientation can be assigned to each point of the street axis, following a similar approach than for the building block facades, and defining also two orientation parameters: azimuth and an orientation label, which in this case can be North–South, East–West, North West–South East, or North East–South West (Figure 5c).

- Context: As contextual information, the indices of the building blocks that are in contact with each street are also stored. Retrieving then is straightforward as this information is already embedded in each street St_i.

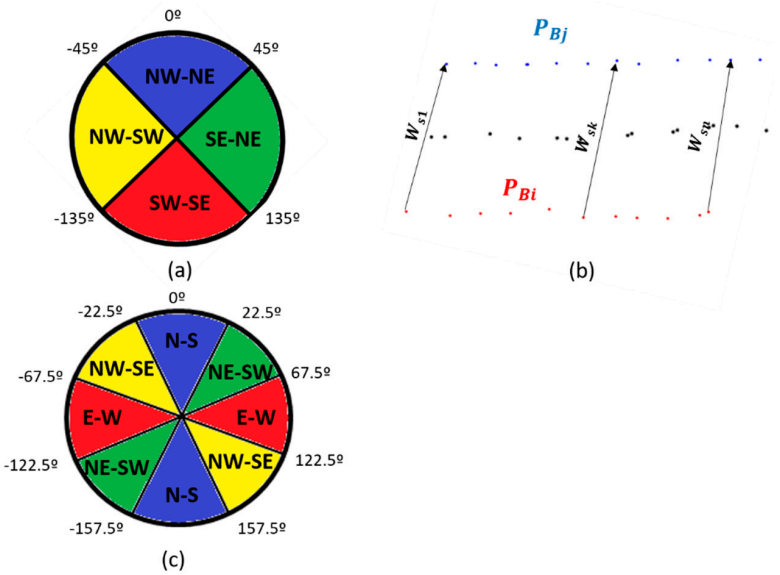

Figure 5. Urban parametrization. (**a**) Façade orientation labels. (**b**) The street width (W_s) is obtained computing the distance between each point in P_{Bi} and the closest point in P_{Bj}. The street axis is obtained averaging each pair of those points. (**c**) Street orientation labels.

Finally, all this information derived from intersections, building blocks, and streets is gathered as properties of objects of custom classes that have been designed to show in an ordered and systematic manner the results of the urban parametrization. The representation of this classes is shown in Figure 6.

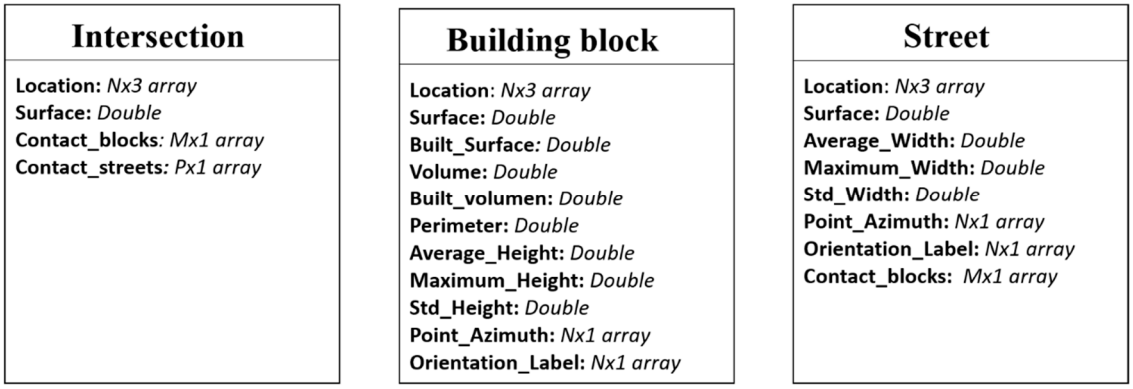

Figure 6. Three different classes with their respective properties are defined for storing information of the intersections, building blocks, and streets.

3. Case Study

The data employed to validate the methodology presented in Section 2 comes from the Spanish National Plan of Aerial Orthophotography (PNOA), which has, among its objectives to offer, point clouds of the whole Spanish territory, using aerial LiDAR sensors. The point clouds collected by the acquisition system have a density of 0.5 pt/m^2 and the average distance between points of 1.4 m. The mean squared error on the vertical direction is $RMSE_Z \leq 0.2$ m. In this work, the case study of Santiago de Compostela, a city in the North-West of Spain, has been considered. This city has three well differentiated urban areas: The historic center, from the 9th century onwards; and two city

expansions, the first one during the 20th century (with a certain urban planning, but with irregular buildings in terms of heights and shapes), and the second one from the first decade of this century (with better planning, more uniformity in the buildings and wider streets). This urban distribution is particularly useful to validate the accuracy of the urban parametrization that is proposed in this work, as it is easy to select point cloud areas that show specific urban characteristics. Table 1 summarizes the point cloud data employed for the validation of the methodology, as well as the coordinates of each urban area (with respect to WGS 84 datum). Three point clouds were manually segmented in order to obtain isolated data for each urban area, as it can be seen in Figure 7.

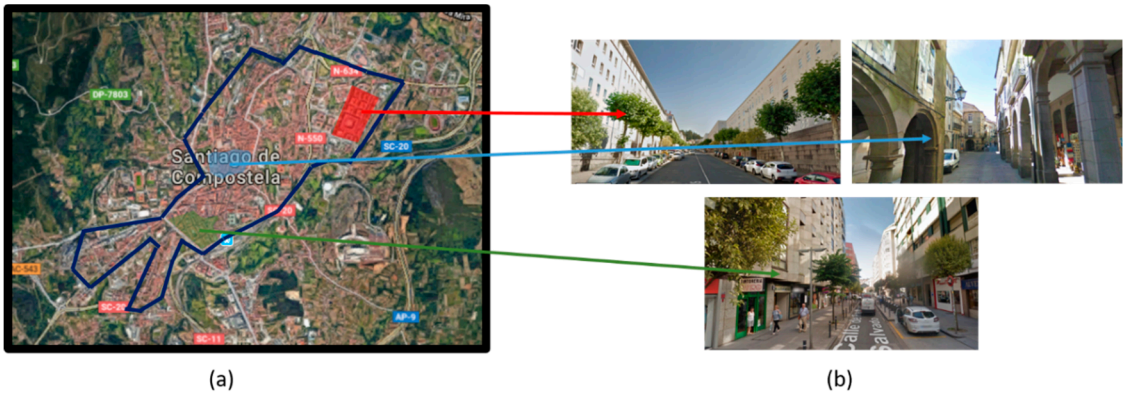

Figure 7. Case study data. Three well-differentiated urban areas from Santiago de Compostela (highlighted in red, green and blue) are chosen for the validation of the proposed methodology.

Table 1. Case study data.

Area	Points	Latitude	Longitude
Santiago City	4,558,644	42°52′49″	8°32′44″
Historic Center	121,514	42°52′41″	8°32′41″
First expansion	213,234	42°52′23″	8°32′59″
Second expansion	203,694	42°53′00″	8°31′37″

4. Results and Discussion

This section shows the results for the urban parametrization of the three areas from the case study of Santiago de Compostela, as presented in Section 3, using the methodology described in Section 2. Furthermore, the accuracy of the measurements is validated by comparing some of the urban parameters with a ground truth.

4.1. Urban Parametrization Results

According to the methodology in Section 2, three different urban elements are parametrized: Intersections, building blocks and streets. Here, the results for the most relevant parameters of each urban element are compared for the three case study areas.

4.1.1. Intersections

The parametrization of the intersections is rather simple, as the only purely geometric parameter that is considered is the surface of the intersection, defined as the area resulting from the triangulation of the points that define it. This will be the only parameter that is being compared for the three case study areas, and the results can be seen in Figure 8. While intersections from the second expansion have, on average, the largest surface and variability, those from the historic center are considerably smaller, which is logical considering that it was not originally built for road traffic.

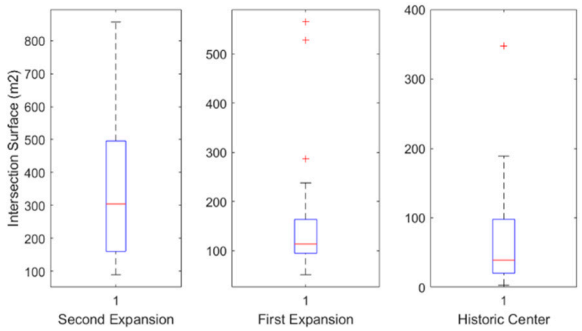

Figure 8. Comparison of intersection surfaces for the three case study areas.

4.1.2. Building Blocks

Regarding building blocks, the following parameters are considered: (1) Surface, (2) Built Surface, (3) Average height, and (4) Facade orientation.

Surface and built surface are compared together in Figure 9a. As can be seen, considering the difference between the average values of area and built area, the presence of interior courtyards is more common in buildings of the second expansion of the city, and almost non-existent in the historic center. Interestingly, there is not a big difference between the surface values in the three areas. The reasoning behind this fact is that building blocks are computed based on building boundaries, hence individual buildings with no physical separation among them will be considered the same building block. That is the case in the historical center, where several smaller buildings are merged as a single building block (Figure 9b).

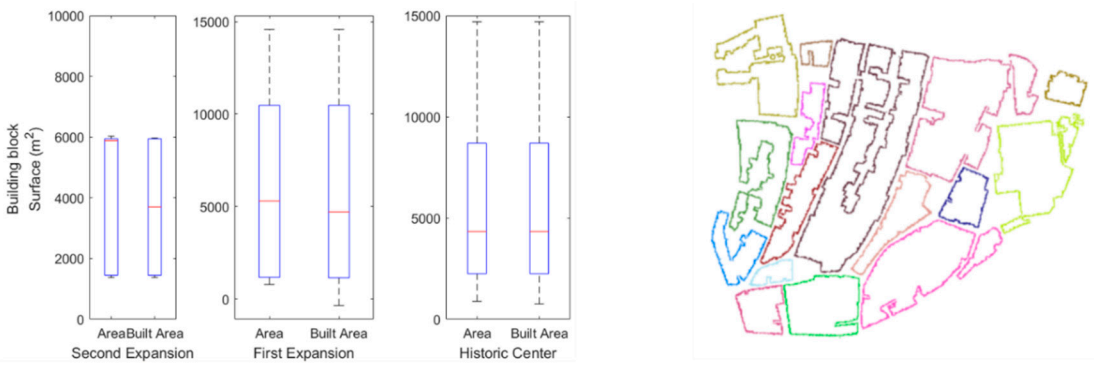

Figure 9. (**a**) Comparison of building block surface and built surface for the three case study areas. (**b**) Although individual buildings are smaller in the city centre, in many cases they are built without physical separation, hence they are considered the same building block, having an impact on the interpretation of the results.

The average building block height as measured using the procedure described in Section 2.5 is shown in Figure 10a. Notice that the first expansion of the city has higher buildings on average, but also presents a larger variability in terms of building height. Buildings from the historic center have also a notable deviation with respect from the average value, which is the lowest value from all three urban areas.

Finally, the orientation of the facades is summarized and compared in Figure 10b. Recall that orientation is defined point-wise using four orientation labels. Here, the percentage of each orientation label is computed for each urban area of the case study. It can be seen that building facades are mainly oriented to the South West–North West and North East–South East, with the exception of the historic center, which has one third of the façade area oriented to the South East–South West.

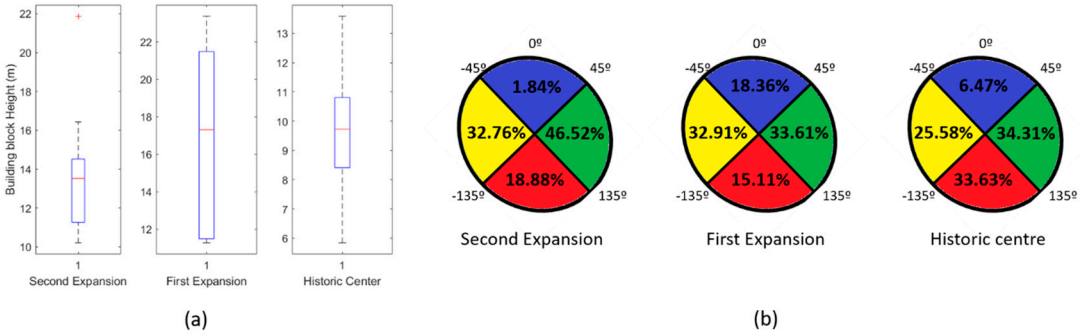

Figure 10. (**a**) Comparison of building block heights for the three case study areas, (**b**) comparison of façade orientation, having in account the four orientation labels that were defined for each point.

4.1.3. Streets

The parameters that are considered for streets are (1) Street surface, (2) Average Width, and (3) Orientation.

Street surface is computed in an analogous way to intersection and building block surfaces, and the results obtained for the three case study areas are shown in Figure 11a. As expected, streets have the largest surface on the second expansion of the city, where the urban planning was more efficient, so there is more surface available for both pedestrians and road traffic; and the smallest in the city center, as it is not meant for the coexistence of pedestrians and vehicles.

Regarding the average street width, the conclusions are similar for the street surface: streets are wider in the modern part of the city and narrower in the historic center (Figure 11b).

Finally, the orientation is measured in an analogous manner than for building blocks (Table 2). The city has grown in the North East–South West direction, therefore the most common orientation of the city expansions is precisely North East–South West, and the perpendicular direction, North West–South East. The historic center presents a different distribution regarding the orientation of the streets. There, the main directions are North–South and East–West. This can be explained by the fact that the historic center has grown around the pathways leading the cathedral, adapting to the topography, which is steeper in the East–West axis.

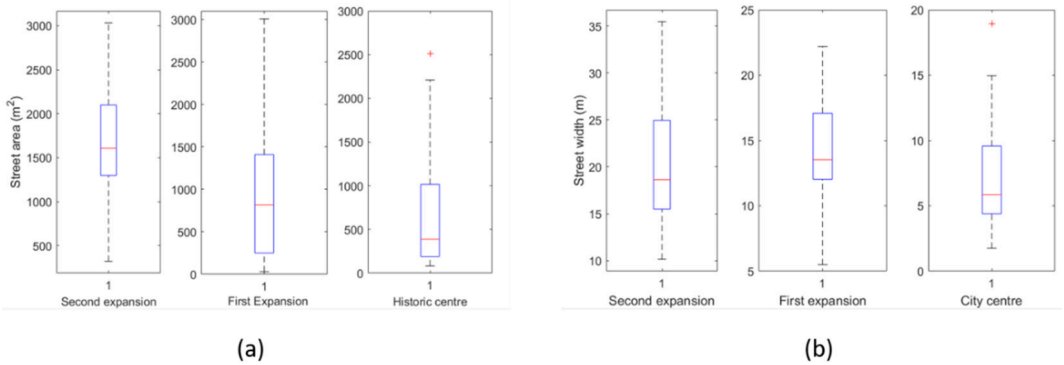

Figure 11. (**a**) Comparison of street areas. (**b**) Comparison of street widths.

Table 2. Comparison of street orientations.

Orientation	% of Points		
	Second Expansion	**First Expansion**	**Historic Centre**
N-S	20.87	12.16	33.33
E-W	12.02	11.35	29.75
NE-SW	31.00	42.10	17.56
NW-SE	36.01	34.39	19.37

4.2. Accuracy Validation

In order to validate the measurements shown in Section 4.1, ground truth data was collected manually to compare some of the urban parameters that are automatically computed with respect to reference data. Specifically, building block surface and perimeter, street width, and intersection surface are the parameters selected for validation. The ground truth was collected using Google Maps, manually measuring each parameter from the urban areas of the case study presented in Section 3. As shown in Figure 12, the manual reference takes into consideration the concept of building block that is defined in Section 2, as an edification or group of edifications that have no physical separation. For this reason, the ground truth only contains reference data from the first and second expansions of the city, as the historic center is a cluttered area in terms of edifications, hence the manual references were collected with inaccuracies that could jeopardize the validation of the results.

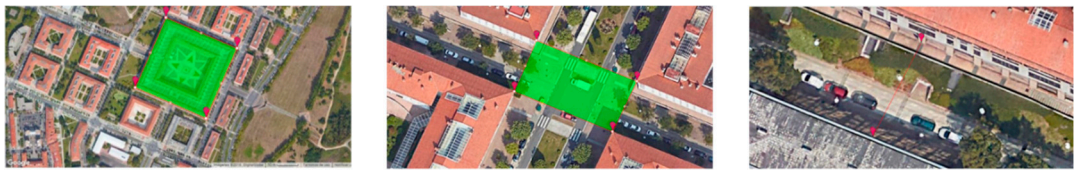

Figure 12. Manual reference. (**a**) Area of a building block. (**b**) Area of an intersection. (**c**) Width of a street.

Tables 3–6 show the results of the comparison between the urban parameters that were automatically extracted from the point cloud data and the manual reference.

In Table 3, the comparison regarding the intersection surface parameter is shown. As can be seen, the measurement error lies consistently around ±3%, averaging less than a 2% error for both of the case study areas that were considered.

Tables 4 and 5 show the comparison for two of the building block parameters: surface and perimeter. Both parameters are accurately measured, also with average errors of around ±3%. The error sources are twofold, (1) The resolution of the point cloud. The average distance between points is 1.4, which introduces inaccuracies in the measurements. (2) The manual collection of ground truth data may include small inaccuracies, as it is done by tracing lines by hand on a Google Maps satellite image. Although this should not affect to the average error, it may have a small influence on individual comparisons between the measured parameters and the ground truth.

Similarly, Table 6 shows the results for the average width of the streets. The errors are in the same interval than the previous parameters, proving that the methodologies that have been developed do not have an impact on the accuracy, and the error can be assumed to be inherent to the accuracy of the point cloud.

Finally, in order to offer a visualization of the results, in Figure 13 building block and street data from the second expansion study area have been exported to Geographic Information System (GIS) shape layers, with a number of parameters related to each element as described in Figure 6.

Table 3. Intersection surface.

First Expansion	Measured Area (m^2)	Ground Truth Area (m^2)	Error (m^2)	Error (%)
	201.71	209.46	−7.75	−3.69
	100.03	103.38	−3.35	−3.24
	113.12	112.11	1.01	0.90
	68.43	66.31	2.12	3.20
	86.82	89.38	−2.56	−2.86
∑	570.11	580.64	**−10.53**	**−1.81**

Table 3. *Cont.*

Second Expansion	Measured Area (m^2)	Ground Truth Area (m^2)	Error (m^2)	Error (%)
	436.27	446.56	−10.29	−2.30
	495.66	510.12	−14.46	−2.83
	677.19	682.08	−4.89	−0.72
	502.69	511.80	−9.11	−1.77
	636.68	640.78	−4.10	−0.64
∑	2748.49	2791.34	**−42.85**	**−1.53**

Table 4. Building block surface.

First Expansion	Measured Area (m^2)	Ground Truth Area (m^2)	Error (m^2)	Error (%)
	5296.10	5005.09	291.01	5.81
	14,582.60	14,166.76	415.84	2.93
	778.59	740.46	38.13	5.14
	1163.7	1117.63	46.07	4.12
	9053.90	8778.82	275.08	3.13
∑	30,874.89	29,808.76	**1066.13**	**3.57**
Second Expansion	**Measured Area (m^2)**	**Ground Truth Area (m^2)**	**Error (m^2)**	**Error (%)**
	35,554.02	34,964.73	589.29	1.68
	5707.54	5540.40	167.14	3.01
	1451.20	1371.90	79.30	5.78
	1442.20	1378.93	63.27	4.59
	1416.80	1363.97	52.83	3.87
∑	45,571.76	44,619.93	**951.83**	**2.13**

Table 5. Building block perimeter.

First Expansion	Measured Perimeter (m)	Ground Truth Area (m)	Error (m)	Error (%)
	380.21	380.31	−0.097	−0.02
	488.38	488.97	−0.59	0.12
	127.42	129.09	−1.67	−1.29
	176.13	178.50	−2.37	−1.33
	386.00	391.26	−5.26	−1.34
∑	1558.14	1568.13	**−9.99**	**−0.64**
Second Expansion	**Measured Perimeter (m)**	**Ground Truth Perimeter (m)**	**Error (m)**	**Error (%)**
	746.31	749.21	−2.90	−0.38
	289.20	297.48	−8.28	−2.78
	178.58	186.64	−8.06	−4.31
	179.40	186.60	−7.20	−3.85
	175.00	185.01	−10.01	−5.41
∑	1568.49	1604.94	**−36.45**	**−2.27**

Table 6. Street width.

First Expansion	Measured Width (m)	Ground Truth Width (m)	Error (m)	Error (%)
	12.80	12.21	0.59	4.83
	13.71	13.55	0.15	1.14
	12.28	12.67	−0.39	−3.07
	13.39	13.95	−0.56	−4.04
	13.48	13.07	0.40	3.09
∑	65.46	65.66	**0.19**	**0.30**
Second Expansion	**Measured Width (m)**	**Ground Truth Width (m)**	**Error (m)**	**Error (%)**
	19.24	18.39	0.84	4.58
	34.51	34.43	0.08	0.24
	25.07	24.96	0.11	0.42
	18.66	18.14	0.51	2.83
	25.44	24.89	0.54	2.19
∑	122.92	120.82	**2.09**	**1.73**

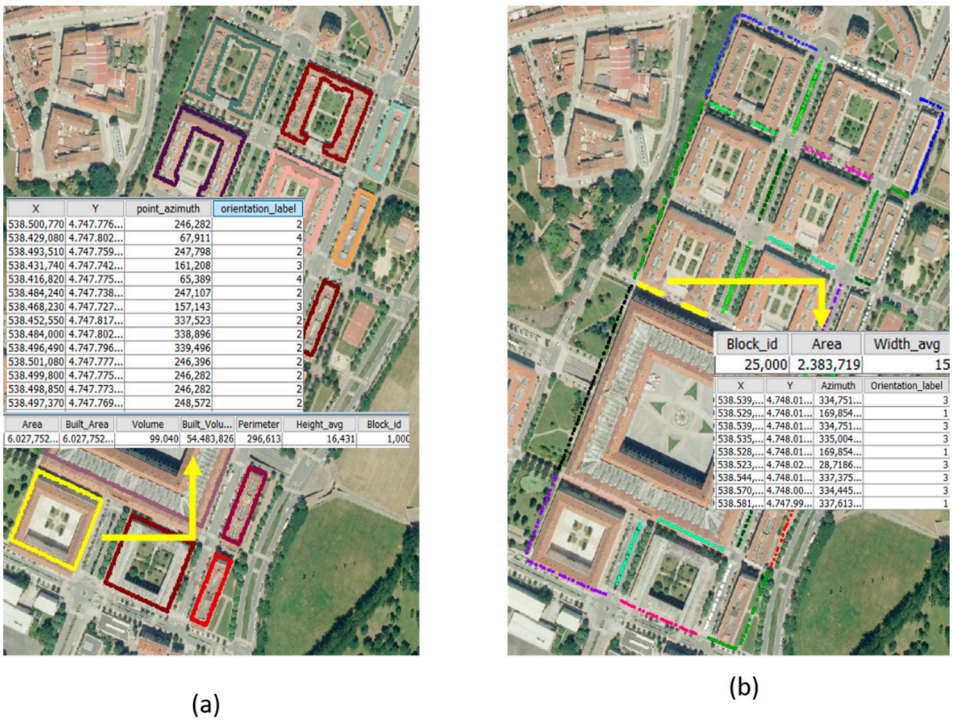

Figure 13. Visualization of the results as a GIS shape layer which overlaps an orthophoto of the case study area. (**a**) Building block parameters can be visualized either point-wise (azimuth and orientation label) or block wise (area, volume, etc.). (**b**) Street parameters can be similarly visualized.

5. Conclusions

In this paper a methodology for the automatic parametrization of urban areas from aerial point clouds is developed for the case study of Santiago de Compostela (Spain). This methodology, which relies only on the geometric parameters of the point cloud (x, y, z coordinates), consists of a number of sequential processes on the point cloud data that aim to detect three of the main elements of the urban structure: building blocks, streets, and intersections. Then, different parameters such as heights, widths, areas, etc. are computed in order to characterize each element. Custom data structures are developed to store this information in a systematic manner.

The case study data was composed of three different urban areas clearly different in terms of urban typology, with the objective of validating the capability of the methodology to distinguish them attending to the extracted urban parameters. The assessment of these parameters showed a clear differentiation on the considered urban typologies, therefore proving that data from the Spanish National Plan of Aerial Orthophotography is suitable for this urban parametrization. Furthermore, the accuracy of the measurements has been also assessed, showing that the errors with respect a manual reference are in the $\pm 3\%$ range, which is acceptable considering the properties of the point cloud in terms of point resolution.

An interesting path for future work could be to focus on the usage of the urban parameters to develop applications related to the automatic classification of urban typologies, or to urban planning in terms of assessing concepts such as the identification of areas with energetic rehabilitation potential, giving decision-making tools to the public administrations in order to prioritize actions. For that purpose, the data that is extracted automatically from the point cloud should be exported to a Geographic Information System (GIS) where it can be combined with different layers of information of the urban environment.

Author Contributions: Conceptualization: A.P.-R.; Methodology and Software: A.P.-R. and M.S.; Validation and Visualization: M.S.; Writing—original draft: A.P.-R. and M.S.; Supervision, Writing—review and editing—and Project Administration: B.R. and P.L.

Funding: This work has been partially supported by Human Resources program FPI (Grant BES-2014-067736), and Xunta de Galicia through grant ED431C2016-038.

Conflicts of Interest: The authors declare no conflict of interest.

References

1. United Nations Human Settlements Programme. *Prosperity of Cities: State of the World's Cities 2012/2013*; United Nations Human Settlements Programme: Nairobi, Kenya, 2012; ISBN 9780415838887.
2. Coppola, P.; Papa, E.; Angiello, G.; Carpentieri, G. Urban form and Sustainability: The Case Study of Rome. *Procedia Soc. Behav. Sci.* **2014**, *160*, 557–566. [CrossRef]
3. Phillis, Y.A.; Kouikoglou, V.S.; Verdugo, C. Urban sustainability assessment and ranking of cities. *Comput. Environ. Urban Syst.* **2017**, *64*, 254–265. [CrossRef]
4. Hawkey, D.; Webb, J.; Winskel, M. Organisation and governance of urban energy systems: District heating and cooling in the UK. *J. Clean. Prod.* **2013**, *50*, 22–31. [CrossRef]
5. Zhang, X.; Li, H. Urban resilience and urban sustainability: What we know and what do not know? *Cities* **2018**, *72*, 141–148. [CrossRef]
6. Dieleman, H. Organizational learning for resilient cities, through realizing eco-cultural innovations. *J. Clean. Prod.* **2013**, *50*, 171–180. [CrossRef]
7. Meerow, S.; Newell, J.P.; Stults, M. Defining urban resilience: A review. *Landsc. Urban Plan.* **2016**, *147*, 38–49. [CrossRef]
8. McCormick, K.; Anderberg, S.; Coenen, L.; Neij, L. Advancing sustainable urban transformation. *J. Clean. Prod.* **2013**, *50*, 1–11. [CrossRef]
9. Capes, R.; Teeuw, R. On safe ground? Analysis of European urban geohazards using satellite radar interferometry. *Int. J. Appl. Earth Obs. Geoinf.* **2017**, *58*, 74–85. [CrossRef]
10. Bathrellos, G.D.; Skilodimou, H.D.; Chousianitis, K.; Youssef, A.M.; Pradhan, B. Suitability estimation for urban development using multi-hazard assessment map. *Sci. Total Environ.* **2017**, *575*, 119–134. [CrossRef] [PubMed]
11. Yousefi, B.; Mirhassani, S.M.; AhmadiFard, A.; Hosseini, M.M. Hierarchical segmentation of urban satellite imagery. *Int. J. Appl. Earth Obs. Geoinf.* **2014**, *30*, 158–166. [CrossRef]
12. Xu, Y.; Ren, C.; Ma, P.; Ho, J.; Wang, W.; Lau, K.K.L.; Lin, H.; Ng, E. Urban morphology detection and computation for urban climate research. *Landsc. Urban Plan.* **2017**, *167*, 212–224. [CrossRef]
13. Tatar, N.; Saadatseresht, M.; Arefi, H.; Hadavand, A. A robust object-based shadow detection method for cloud-free high resolution satellite images over urban areas and water bodies. *Adv. Space Res.* **2018**, *61*, 2787–2800. [CrossRef]
14. Puente, I.; González-Jorge, H.; Martínez-Sánchez, J.; Arias, P. Review of mobile mapping and surveying technologies. *Meas. J. Int. Meas. Confed.* **2013**, *46*, 2127–2145. [CrossRef]
15. Yang, B.; Dong, Z.; Zhao, G.; Dai, W. Hierarchical extraction of urban objects from mobile laser scanning data. *ISPRS J. Photogramm. Remote Sens.* **2015**, *99*, 45–57. [CrossRef]
16. Golovinskiy, A.; Kim, V.G.; Funkhouser, T. Shape-based recognition of 3D point clouds in urban environments. In Proceedings of the 2009 IEEE 12th International Conference on Computer Vision, Kyoto, Japan, 29 September–2 October 2009. [CrossRef]
17. Serna, A.; Marcotegui, B. Detection, segmentation and classification of 3D urban objects using mathematical morphology and supervised learning. *ISPRS J. Photogramm. Remote Sens.* **2014**, *93*, 243–255. [CrossRef]
18. Yu, Y.; Li, J.; Guan, H.; Wang, C.; Yu, J. Semiautomated Extraction of Street Light Poles from Mobile LiDAR Point-Clouds. *IEEE Trans. Geosci. Remote Sens.* **2015**, *53*, 1374–1386. [CrossRef]
19. Janowski, A.; Nierebinski, P.; Szulwic, J. Artificial Model in the Assessment of the Algorithm of Objects Recorded by Laser Scanning Shape Detection (Als/Tls). In Proceedings of the 15th International Multidisciplinary Scientific GeoConference SGEM 2015, Albena, Bulgaria, 18–24 June 2015; Volume 1, pp. 995–1002. [CrossRef]
20. Díaz-Vilariño, L.; González-Jorge, H.; Bueno, M.; Arias, P.; Puente, I. Automatic classification of urban pavements using mobile LiDAR data and roughness descriptors. *Constr. Build. Mater.* **2016**. [CrossRef]
21. Xia, S.; Wang, R. Extraction of residential building instances in suburban areas from mobile LiDAR data. *ISPRS J. Photogramm. Remote Sens.* **2018**, *144*, 453–468. [CrossRef]

22. Guan, H.; Li, J.; Yu, Y.; Wang, C.; Chapman, M.; Yang, B. Using mobile laser scanning data for automated extraction of road markings. *ISPRS J. Photogramm. Remote Sens.* **2014**, *87*, 93–107. [CrossRef]
23. Yu, Y.; Li, J.; Wen, C.; Guan, H.; Luo, H.; Wang, C. Bag-of-visual-phrases and hierarchical deep models for traffic sign detection and recognition in mobile laser scanning data. *ISPRS J. Photogramm. Remote Sens.* **2016**, *113*, 106–123. [CrossRef]
24. Yan, J.; Shan, J.; Jiang, W. A global optimization approach to roof segmentation from airborne lidar point clouds. *ISPRS J. Photogramm. Remote Sens.* **2014**, *94*, 183–193. [CrossRef]
25. Soilán, M.; Riveiro, B.; Liñares, P.; Padín-Beltrán, M. Automatic Parametrization and Shadow Analysis of Roofs in Urban Areas from ALS Point Clouds with Solar Energy Purposes. *Int. J. Geo-Inf.* **2018**, *7*. [CrossRef]
26. Rahman, M.T.; Rashed, T. Urban tree damage estimation using airborne laser scanner data and geographic information systems: An example from 2007 Oklahoma ice storm. *Urban For. Urban Green.* **2015**, *14*, 562–572. [CrossRef]
27. Holopainen, M.; Kankare, V.; Vastaranta, M.; Liang, X.; Lin, Y.; Vaaja, M.; Yu, X.; Hyyppä, J.; Hyyppä, H.; Kaartinen, H.; et al. Tree mapping using airborne, terrestrial and mobile laser scanning—A case study in a heterogeneous urban forest. *Urban For. Urban Green.* **2013**, *12*, 546–553. [CrossRef]
28. Hermosilla, T.; Palomar-Vázquez, J.; Balaguer-Beser, Á.; Balsa-Barreiro, J.; Ruiz, L.A. Using street based metrics to characterize urban typologies. *Comput. Environ. Urban Syst.* **2014**, *44*, 68–79. [CrossRef]
29. Vanderhaegen, S.; Canters, F. Mapping urban form and function at city block level using spatial metrics. *Landsc. Urban Plan.* **2017**, *167*, 399–409. [CrossRef]
30. Gressin, A.; Mallet, C.; Demantké, J.; David, N. Towards 3D lidar point cloud registration improvement using optimal neighborhood knowledge. *ISPRS J. Photogramm. Remote Sens.* **2013**, *79*, 240–251. [CrossRef]
31. Fortune, S. Voronoi diagrams and Delaunay triangulations. *Comput. Euclidean Geom.* **1992**, *1*, 2. [CrossRef]
32. Reddy, P.R.; Amarnadh, V.; Bhaskar, M. Evaluation of Stopping Criterion in Contour Tracing Algorithms. *Int. J. Comput. Sci. Inf. Technol.* **2012**, *3*, 3888–3894.
33. Soilán, M.; Truong-hong, L.; Riveiro, B.; Laefer, D. Automatic extraction of road features in urban environments using dense ALS data. *Int. J. Appl. Earth Obs. Geoinf.* **2018**, *64*, 226–236. [CrossRef]